Mechanical properties of thermally damaged mortar under coupled static-dynamic loading

Chengjuan Ying[1], Haiming Chen[2]*, Jie Chen[2], Liangxiao Xiong[3] and Duoxi Yao[1]

[1]School of Earth and Environment, Anhui University of Science and Technology, Huainan, China, [2]Engineering Research Center of Underground Mine Construction, Ministry of Education, Anhui University of Science and Technology, Huainan, China, [3]School of Civil Engineering and Architecture, East China Jiaotong University, Nanchang, China

In buildings that experience fires, cement mortar is subjected to high-temperature environments and not only the weight of the structure above but also blast loads, leading to structural damage and loss of load-bearing capacity. To investigate the static and dynamic mechanical properties of thermally damaged mortar, a series of tests utilizing modified split Hopkinson pressure bar were conducted. These tests included quasi-static, conventional dynamic and coupled static-dynamic loading tests on mortar specimens that were subjected to seven temperature levels: 20°C, 100°C, 200°C, 300°C, 400°C, 500°C, and 600°C. The test results revealed that both the thermal damage and loading method had an impact on the mechanical properties and damage characteristics of the mortar specimens. The compressive strength, elastic modulus and absorbed energy ratio of mortar decreased as temperature increased. Notably, the quasi-static strength loss rate was 60% when the temperature reached 600°C. Under coupled static-dynamic loading, the specimens exhibited higher strength, elastic modulus, reflected energy ratio, and transmitted energy ratio. Conversely, they had lower average strain rates and absorbed energy ratios. Intriguingly, the dynamic growth factor had a relative increase of 0.7−2.0 compared with other loading methods. Furthermore, the higher temperature, the higher fragmentation of the specimens in the fragmentation pattern. Conventional dynamic loading resulted in the greatest degree of fragmentation. The findings provide a scientific basis for the design and evaluation of concrete shockproof and explosion-resistant structures.

KEYWORDS

mechanical properties, thermal damage, mortar, coupled static-dynamic loading, energy dissipation

1 Introduction

Cement mortar was widely utilized in various architectural structures, including buildings, bridges, and tunnels. In modern times, the complex layout of building pipelines and dense urban landscapes had increased the likelihood and severity of fire, resulting in substantial economic losses (Aitcin, 2003; Hertz, 2005; Liu et al., 2020). Fire posed significant threats to individuals' safety and property, with fire losses in China steadily rising. Fires caused severe damage to the building materials, resulting in a decrease in the structure's load-bearing capacity (Schrefler et al., 2002; Patrick and Pietro, 2014). During a fire incident, the upper building structure experienced high-temperature failure,

while the lower structure was impacted by falling debris, accompanied by the explosive effects of explosive materials. Cementitious materials were subjected to a combination of high temperature and various types of loading failure, ultimately leading to building collapse, posing a significant threat to the safety of individuals and property (Khoury, 2000; Annerel and Taerwe, 2009; Du et al., 2018). Therefore, to further understand the mechanical properties of cement mortar in abnormal environments, it was essential to evaluate the residual properties after thermal damage (Lu et al., 2013; Mukesh and Shashank, 2019; Zhao et al., 2019).

During fire, the simultaneous occurrence of thermal damage and various forms of loading on cement mortar often led to the destruction of the concrete structures (Biolzi, Cattaneo, and Rosati, 2008). Recent studies primarily focused on investigating the static mechanical properties of thermally damaged cement-based materials. Cree, Green, and Noumowé (2013) carried out quasi-static strength tests on thermally damaged cement mortar and concrete, and established typical strength loss model. Bamonte, Gambarova, and Sciarretta (2021) investigated the mechanical properties of mortars after heating to 200, 400 and 600°C and 900°C to evaluate the thermal diffusion coefficient. Jeyaprabha, Elangovan, and Prakash (2016) placed mortar mixtures at temperatures of 200°C, 500°C, 700°C, and 900°C, followed by cooling with water, and measured their compressive strength. Yazıcı, Sezer, and Şengül (2012) investigated the effect of subjecting mortars to temperature ranging from 20°C to 750°C in a ceramic furnace for 1 h on their compressive strength. Zhang et al. (2000) investigated the effects of high temperature duration and curing age on the energy parameters, strength parameters, stiffness parameters, and brittleness parameters of ordinary and high-strength thermally damaged concrete. It was found that these properties generally decreased linearly with increasing temperature. Deng et al. (2020) studied the mechanical properties of recycled aggregate concrete after thermal temperature to provide scientific guidance for the design of recycled concrete fire protection. In addition, some scholars had studied the static-dynamic behaviors of concrete. Chen et al. (2019); Luo et al. (2020) studied the static-dynamic mechanical properties of concrete columns in order to provide reference for earthquake resistance and disaster reduction.

Concrete was susceptible to high temperatures and blast or impact loads. Therefore, the effect of thermal damage on the dynamic mechanical properties of concrete was crucial. However, there was little research on the behavior of cement mortar under the combination of high temperature and impact loads. Bi et al. (2020) found water cooling produced more irregular fragments and smaller fragments than air cooling at the same temperature and strain rate during the dynamic test of concrete. Yao et al. (2017) studied the mortar's dynamic compressive strength treated temperatures ranging from 150°C to 850°C, quantified thermal damage based on microcracks and chemical changes, and developed a dynamic uniaxial loading model with temperature and strain rate effects using damage variables. This model predicted the strength of mortar after high temperatures.

However, there is a lack of research on mechanical properties of thermally damaged cement mortar under different loading forms, especially under coupled static-dynamic loading. In this study,

mortar was first heated to temperatures of 100°C, 200°C, 300°C, 400°C, 500°C, and 600°C, and then naturally cooled. Subsequently, quasi-static, dynamic and coupled static-dynamic loading tests were conducted using a modified SHPB device. The effects of different loading modes on the mechanical properties, damage morphology, and energy dissipation characteristics of the thermally damaged cement mortar were discussed. It was found that when the temperature reached 600°C, the quasi-static strength loss rate was about 60%, and the strength increased under static-dynamic loading. The results of this study will help further understand the effects of different loading methods on dynamic strength and deformation characteristics of thermally damaged mortar, reveal the damage law and dynamic damage mechanism of mortar after high-temperature damage. The research results will provide scientific basis for improving the fire safety performance of buildings and evaluating fire accidents.

2 Materials and methods

2.1 Materials

P·O 42.5 cement was produced from Huainan Conch Cement Co., Ltd. in Huainan city in this study. The natural river sand was collected from the Huaihe River region of China, and had a fine grain modulus of 2.36 and an apparent density of 2,550 kg/m^3. The water was taken from the laboratory tap. The chemical compositions of cement are presented in Table 1.

2.2 Sample preparation

The water-binder ratio of the mortar used in this study was 0.38, and the ratio of binder to sand was 1:1.2 (Xiong and Chen, 2020). Different loading tests were conducted on specimens with a diameter of 50 mm and height of 50 mm, following the method described in the reference by Zhou et al. (2012). The specimens were cured for 28 days after casting. The test program is presented in Table 2.

2.3 Methods

2.3.1 Thermal treatments
To prevent the rapid evaporation of water in the Muffle furnace from damaging the furnace wall, the specimens were dried in a 105°C oven for 1 day. They were heated to temperatures of 100°C, 200°C, 300°C, 400°C, 500°C and 600°C at a rate of 6°C/min after completely cooled. Each temperature was maintained for 120 min to ensure uniform temperature distribution within the specimens then cooled in the furnace before further testing (Gao et al., 2023). A group of nine specimens were used at each temperature. The SX2-8-10A resistance furnace manufactured by the Shangyu Daoxu Scientific Instrument Co., Ltd. in Shaoxing city was utilized in the study. The thermal cycle temperature curve of high-temperature treatment is shown in Figure 1.

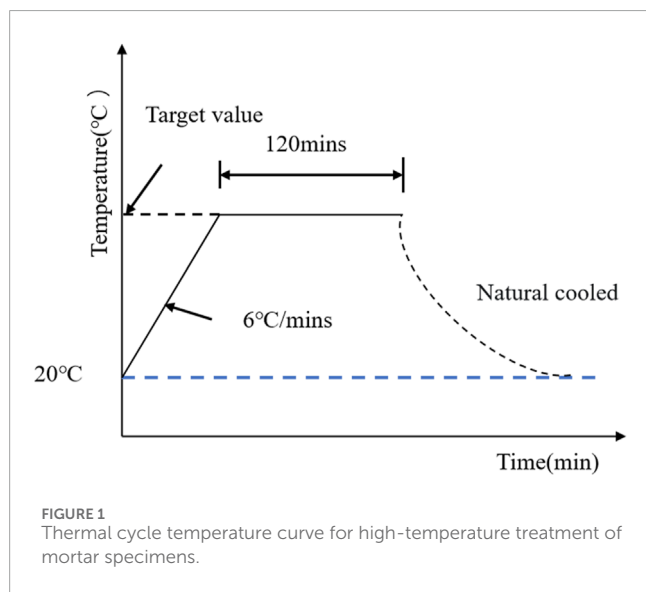### 2.3.2 Quasi-static loading test
The quasi-static compressive strength of the mortar was determined using a DYE-300 universal testing machine. The loading

TABLE 1 Chemical compositions of cement (wt%).

Material	CaO	SiO$_2$	Fe$_2$O$_3$	Al$_2$O$_3$	MgO	SO$_3$	LOI
Cement	49.7	30.6	3.4	7.8	3.7	3.7	1.1

TABLE 2 Test program.

Group (S)	Thermal temperature	Loading condition	Group	Thermal temperature	Loading condition	Group	Thermal temperature	Loading condition
T20	20	Quasi-static	T20D	20	Dynamic	T20SD	20	Static-dynamic
T100	100		T100D	100		T100SD	100	
T200	200		T200D	200		T200SD	200	
T300	300		T300D	300		T300SD	300	
T400	400		T400D	400		T400SD	400	
T500	500		T500D	500		T500SD	500	
T600	600		T600D	600		T600SD	600	

FIGURE 1
Thermal cycle temperature curve for high-temperature treatment of mortar specimens.

rate during the tests was controlled to be approximately 1 kN/s. Three specimens were tested at each thermal treatment temperature.

2.3.3 Dynamic loading test

The dynamic loading tests were conducted using a SHPB device with 50 mm diameter to apply an impact air pressure of 0.3 MPa. The SHPB device, as shown in Figure 2, can also be used for coupled static-dynamic loading tests. The launcher consists of a launch cavity and a spindle-shaped bullet, while the incident and transmitted rods possess an elastic modulus of 210 GPa and a wave propagation velocity of 5,200 m/s. To reduce the radial inertia between the specimens and the rods during dynamic loading,

petroleum jelly was uniformly coated on the cross sections of the incident and transmitted rods. The loading applied on the specimens were determined according to the one-dimensional stress wave propagation theory. It was assumed that stress in SHPB was in state of equilibrium. The stress, strain rate, and strain were calculated by Eqs (1)–(3) (Jiang et al., 2023):

$$\sigma = \frac{A_0 E_0}{A_s} \varepsilon_T \qquad (1)$$

$$\dot{\varepsilon} = -\frac{2C_0}{l_s} \varepsilon_R \qquad (2)$$

$$\varepsilon = -\frac{2C_0}{l_s} \int_0^t \varepsilon_R \mathrm{d}t \qquad (3)$$

where E_0, A_0 and C_0 are the elastic modulus, cross-sectional area and longitudinal wave velocity of the bar, respectively; A_s and l_s are the cross-sectional area and length of cement mortar specimens, respectively; ε_T and ε_R are the transmitted and reflected strain on the rod, respectively.

2.3.4 Coupled static-dynamic loading test

The test was conducted using the device in Figure 2. Mortar was performed static-dynamic loading tests with an impact air pressure of 0.3 MPa. In this case, an axial load was applied prior to the impact (Dai et al., 2010), with the magnitude of the axial load being 10% of the quasi-static compressive strength after thermal treatment. The impact dynamic loads were applied by opening the valve and releasing the bullet after a stabilization period of 5s for the axial load indication.

2.3.5 Scanning electron microscope (SEM) test

SEM tests were conducted to investigate the microstructure and morphology of thermally damaged cement mortar's hydration

FIGURE 2
Improved SHPB for dynamic and static-dynamic loading tests.
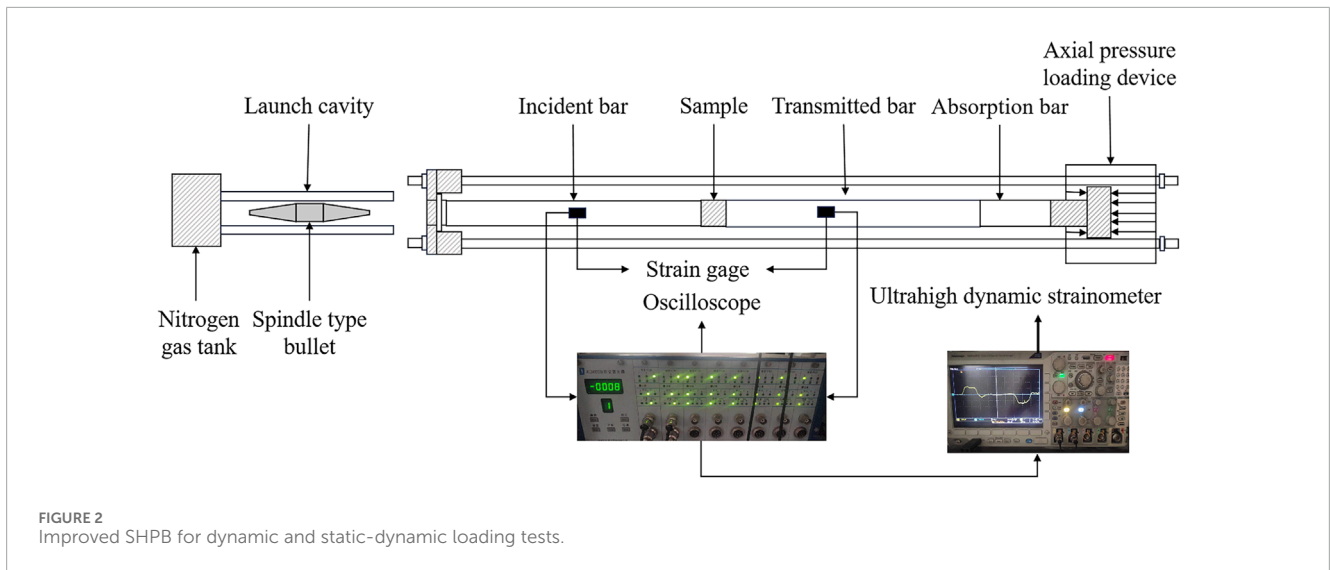
products. This test utilized a Flex1000 electron microscope scanner. The loaded specimens were crushed and sampled, followed by continuous pumping for 24 h in a vacuum pump. Subsequently, they were sprayed with gold, and the SEM images were recorded.

3 Results and discussion

3.1 Mechanical properties of thermally damaged mortar under different loading conditions

Based on the assumption of one-dimensional stress wave theory, the dynamic stress in incident rod is equal to the dynamic stress in the transmitted rod. The results of stress balance tests conducted on specimens are presented in Figure 3, which reveals that the sum of the incident and reflected dynamic stresses was equal to the transmitted dynamic stress. This confirms that the dynamic stresses on both sides of specimens were balanced, thereby ensuring the reliability of the data.

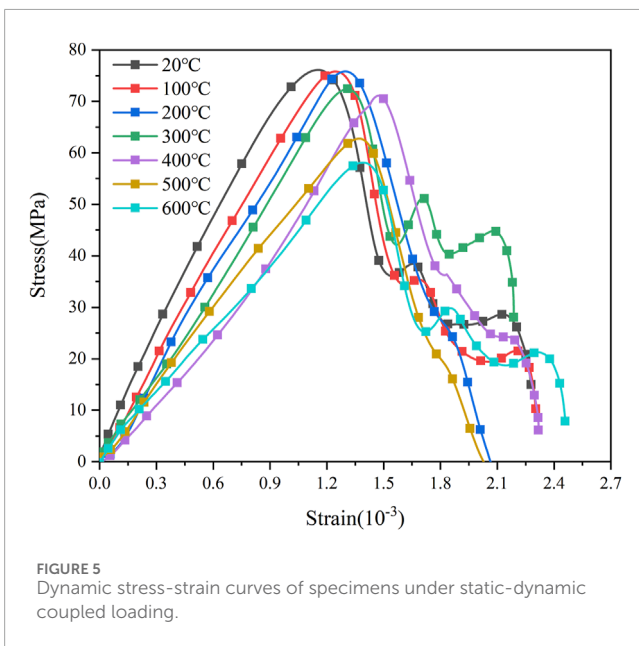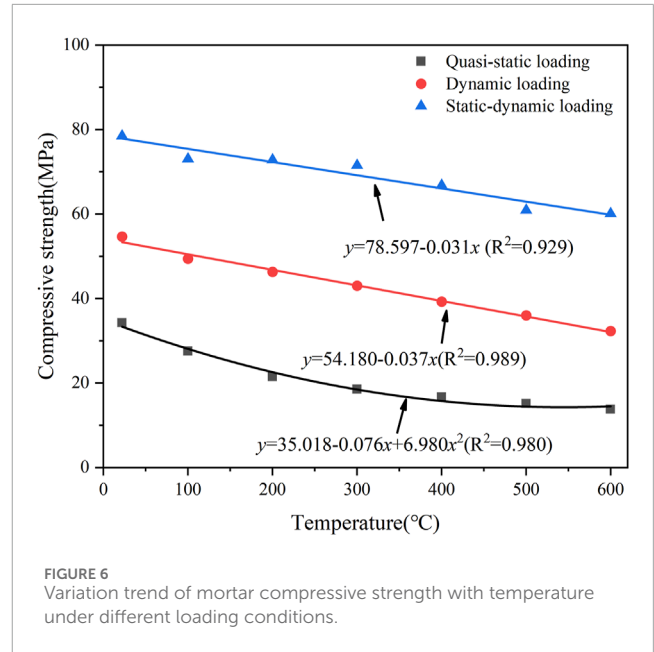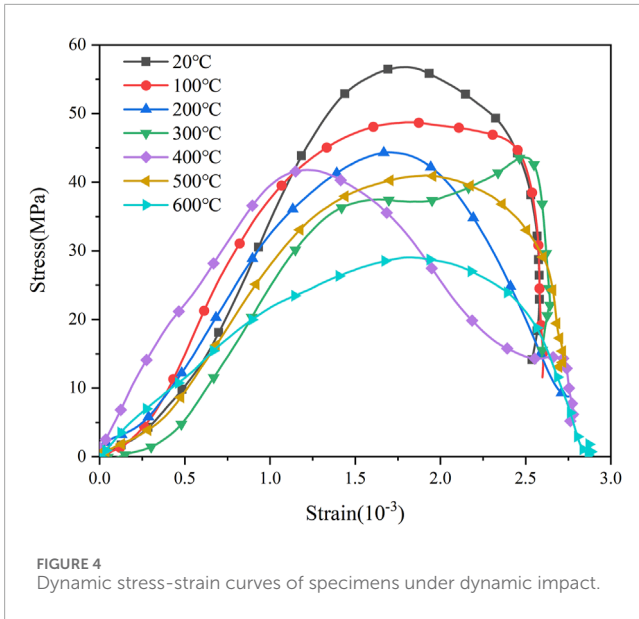### 3.1.1 Dynamic stress-strain curve characteristics
To investigate the effect of thermal damage and different loadings on stress-strain curve characteristics of mortar specimens, typical mortar specimens with compressive strength closest to the average value were selected for further analysis. Figures 4, 5 illustrate the stress-strain curves of thermally damaged specimens under dynamic loading and coupled static-dynamic loading, respectively, which can be divided into three stages.

Stage 1: The elastic deformation stage was characterized by approximately linear growth of mortar stress with strain, a stable dynamic elastic modulus (E_c). The E_c was found to be dependent on the high temperature, with the control group exhibiting the highest value of E_c. However, when the temperature reached 600°C, the E_c was the smallest. At this stage, micro-pores were present within the mortar specimens, and micro-cracks formed between sand particles and cementitious material. These cracks experienced

FIGURE 3
Dynamic stress equilibrium curves of mortar specimens during the dynamic loading tests.
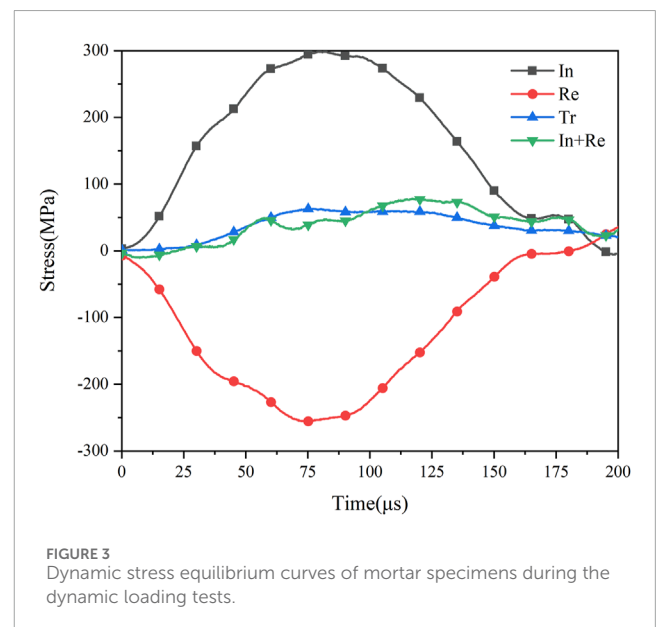
extrusion and shrinkage. Nevertheless, due to the pre-applied axial load during static-dynamic loading tests, this stage was shorter in duration, resulting in higher compactness and a relatively smaller peak strain.

Stage 2: The plastic deformation stage was characterized by a change in the dynamical mechanical properties after the elastic limit stress was reached. As deformation increased, the plastic deformation stage under dynamic loading became more pronounced, while that under coupled static-dynamic loading was shorter. Upon reaching the yield stress, the strain of the specimens increased to a certain extent, but the stress decreased sharply. This phenomenon can be attributed to the axial loading compacting the internal structure of the mortar, thereby exacerbating the damage caused by thermal damage to the specimens.

FIGURE 4
Dynamic stress-strain curves of specimens under dynamic impact.

FIGURE 6
Variation trend of mortar compressive strength with temperature under different loading conditions.

FIGURE 5
Dynamic stress-strain curves of specimens under static-dynamic coupled loading.

Stage 3: The unloading stage was characterized by the rapid decrease in the stress of the specimens under dynamic loading when their internal damage has accumulated to the limit of fracture. Inversely, mortar subjected to static-dynamic loading exhibited one or more secondary stress peaks, indicating that they still possessed a certain load-bearing capacity after damage and had not completely broken down.

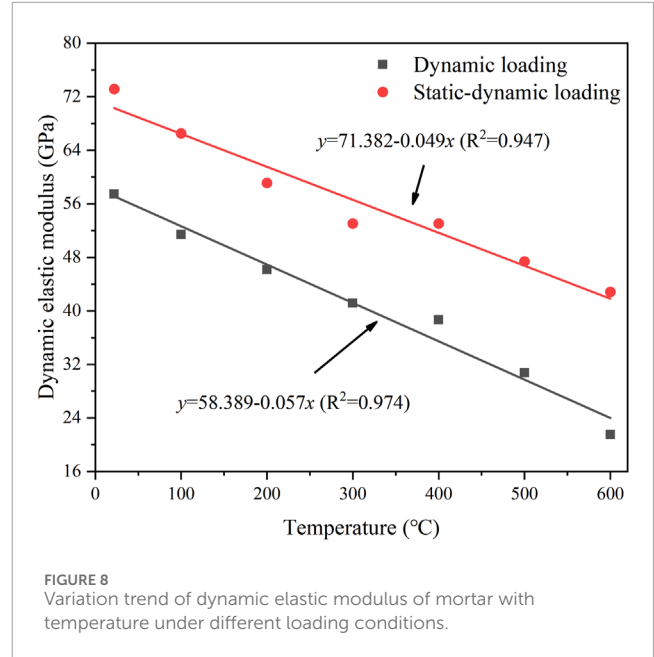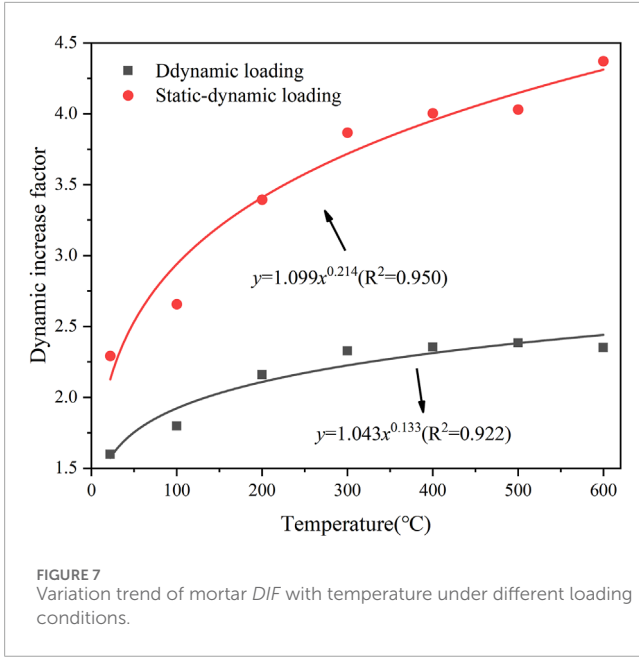### 3.1.2 Compressive strength characteristics

The impact of high-temperature on compressive strength of thermally damaged mortar was a crucial factor that must be considered. As illustrated in Figure 6, it can be observed that the compressive strength of thermally damaged mortar decreased

with temperature under the same loading conditions. The quasi-static compressive strength (σ_s) exhibited a quadratic function trend with temperature, resulting in a correlation coefficient R^2 of 0.980. In contrast, the dynamic compressive strength (σ_d) of mortar under dynamic and static-dynamic loading displayed a linear downward trend, with correlation coefficients R^2 of 0.989 and 0.929, respectively. The results clearly indicated that the compressive strength of mortar was the highest under static-dynamic loading, followed by that under dynamic loading, and lowest under quasi-static loading.

The dynamic increase factor (*DIF*) is defined as the ratio of the average σ_d to the average σ_s for thermally damaged specimens. It is commonly used to assess and compare the influence of impact loads on material strength (Xu and Li, 2011; Yao et al., 2016; Yin et al., 2018; Shu et al., 2022). Variation trend of mortar *DIF* with temperature under different loading conditions is illustrated in Figure 7. Under the same loading conditions, *DIF* increased approximately exponentially with temperature, with correlation coefficients R^2 reaching 0.922 and 0.950, respectively. When axial static pressure and dynamic loading were combined, static pressure caused compaction of the pores, leading to a significant increase in *DIF* (from 0.7 to 2.0). In summary, *DIF* is sensitive to variations in high temperature and pre-applied axial pressure.

3.1.3 Deformation characteristics

Dynamic elastic modulus E_c is a measure of the deformation ability of a specimen under elastic deformation. The corresponding strain is the peak strain when the specimen reaches its peak stress (Chen et al., 2022; Li et al., 2023; Michał et al., 2023; Zhang et al., 2023). The elastic modulus of mortar was determined by selecting the slopes of the tangents at two points on the stress-strain curve, namely, when the stress reached 0.3 times and 0.6 times the peak

FIGURE 7
Variation trend of mortar *DIF* with temperature under different loading conditions.

FIGURE 8
Variation trend of dynamic elastic modulus of mortar with temperature under different loading conditions.

stress σ_{max}. The calculation formula is Eq. (4):

$$E_c = \frac{\sigma_1 - \sigma_2}{\varepsilon_1 - \varepsilon_2} \qquad (4)$$

where σ_1 and σ_2 are the stresses at the two points corresponding to 0.6 times σ_{max} and 0.3 times σ_{max} on the stress-strain curve, respectively; ε_1 and ε_2 are the strains at the two points, respectively.

The relationship between E_c of mortar and temperature is shown in Figure 8. E_c decreased linearly with increasing of temperature, with correlation coefficients R^2 of 0.974 and 0.947, respectively. E_c of mortar under dynamic loading and static-dynamic loading at 600°C decreased by 62.58% and 41.44%, respectively, compared to that at 20°C. This reduction was due to the same reason as the decrease in dynamic compressive strength.

3.1.4 Strain rate characteristic

The relationship between the average strain rate and temperature is illustrated in Figure 9. The strain rate of mortar under dynamic loading and static-dynamic loading increased linearly with increasing temperature, with correlation coefficients R^2 of 0.913 and 0.927, respectively. The strain rate of mortar under static-dynamic loading was lower than that under dynamic loading. The strain rate of mortar under dynamic loading ranged from 143.96 to 151.57 s^{-1}, while that under static-dynamic loading ranged from 112.44 to 126.19 s^{-1}. Due to the pre-applied axial load, the structure of mortar became denser, σ_d increased, the peak strain decreased.

3.2 Failure pattern of thermally damaged mortar under different loading conditions

3.2.1 Fracture morphology and failure mode

The mortar failure pattern is closely related to the fragments of the specimens after loading (Shuai et al., 2020; Padmanabha et al.,

FIGURE 9
Variation trend of average strain rate of mortar with temperature under different loading conditions.
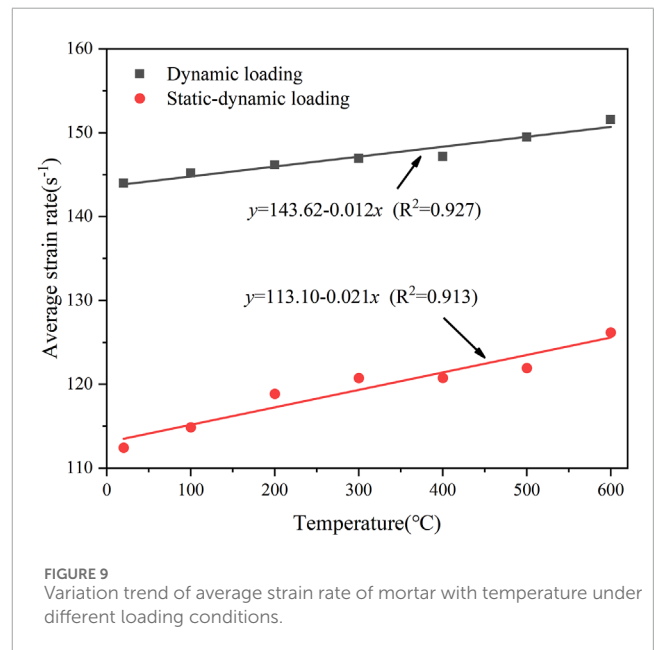
2022; Zheng et al., 2023). As observed from Table 3, as the temperature increased from 20°C to 600°C, the mortar color changed from the usual gray to off-gray and then to pale yellow. As the temperature increased, the thermally damaged mortar became powderier and the degree of fragmentation also increased. Under different loading conditions, the mortar specimens subjected to SHPB impact broke into blocky pieces. Compared with specimens under static-dynamic loading, those under dynamic loading exhibited more irregular and smaller fragmentation. This was because the axial pressure made the pores of mortar denser and the coupled effect of static-dynamic loading enhanced its compressive strength. Despite varying thermal damage

TABLE 3 Typical fracture morphology of mortar.

Loading condition	Thermal temperature (°C)			
	20	200	400	600
Quasi-static				
Dynamic				
Static-dynamic				

temperatures and different forms of loading conditions, the failure mode of the mortar remained consistent - splitting and tensile failure.

3.2.2 Facture surface

The SEM tests were conducted on the thermally damaged mortar specimens (Figure 10). The compressive strength loss of thermally damaged mortar was closely related to the mass loss (Figure 11). With the increased temperature, the number of cracks and pores on the fracture surface gradually increased. The mass loss rate and quasi-static compressive strength loss rate increased exponentially with temperature, with correlation coefficients of 0.952 and 0.926, respectively. In Figure 10A, the gel structure in the mortar was intact at 20°C, and the dense calcium hydroxide was very neat and complete. At temperatures between 100 and 110°C, free water escaped from the cement mortar, and the hydrated calcium silicate gel began to dehydrate. The hydrated calcium aluminate began to dehydrate around 200°C (Li et al., 2012; Chen et al., 2023). At temperature of 300°C, the mass loss rate was about 5%, while the strength loss rate was about 40%. At this stage, the primary cause of damage to the mortar was the micropores and microcracks shown in Figure 10B (Chen et al., 2023; Yu et al., 2023). As the temperature surpassed 300°C, the number of microcracks and pores in Figure 10C increased. Upon reaching a temperature of 600°C, numerous microcracks and pores became evident at the interface, as depicted in Figure 10D (Min-Ho and Sang-Jin, 2006;

Faisal et al., 2018). The maximum strength loss rate of mortar reached 60%, while the mass loss rate increased to approximately 8%. The decomposition temperature range for calcium carbonate in the cement paste was 850°C–900°C (Son and William, 2014; Stoyanov et al., 2023).

3.2.3 Energy dissipation of thermally damaged mortar under dynamic and coupled static-dynamic loading

Equations (5)–(8) for calculating energy dissipation are as follows:

$$E_I = E_0 C_0 A_0 \int_0^t \varepsilon_T^2 \, dt \tag{5}$$

$$E_R = E_0 C_0 A_0 \int_0^t \varepsilon_T^2 \, dt \tag{6}$$

$$E_T = E_0 C_0 A_0 \int_0^t \varepsilon_T^2 \, dt \tag{7}$$

$$E_A = E_I - E_R - E_T \tag{8}$$

where, $E_I(t)$, $E_R(t)$, $E_T(t)$, and $E_A(t)$ are the incident energy, reflected energy, transmitted energy, and absorbed energy, respectively.

Under different loading conditions, the energy dissipation law of mortar specimens was investigated by using energy ratio
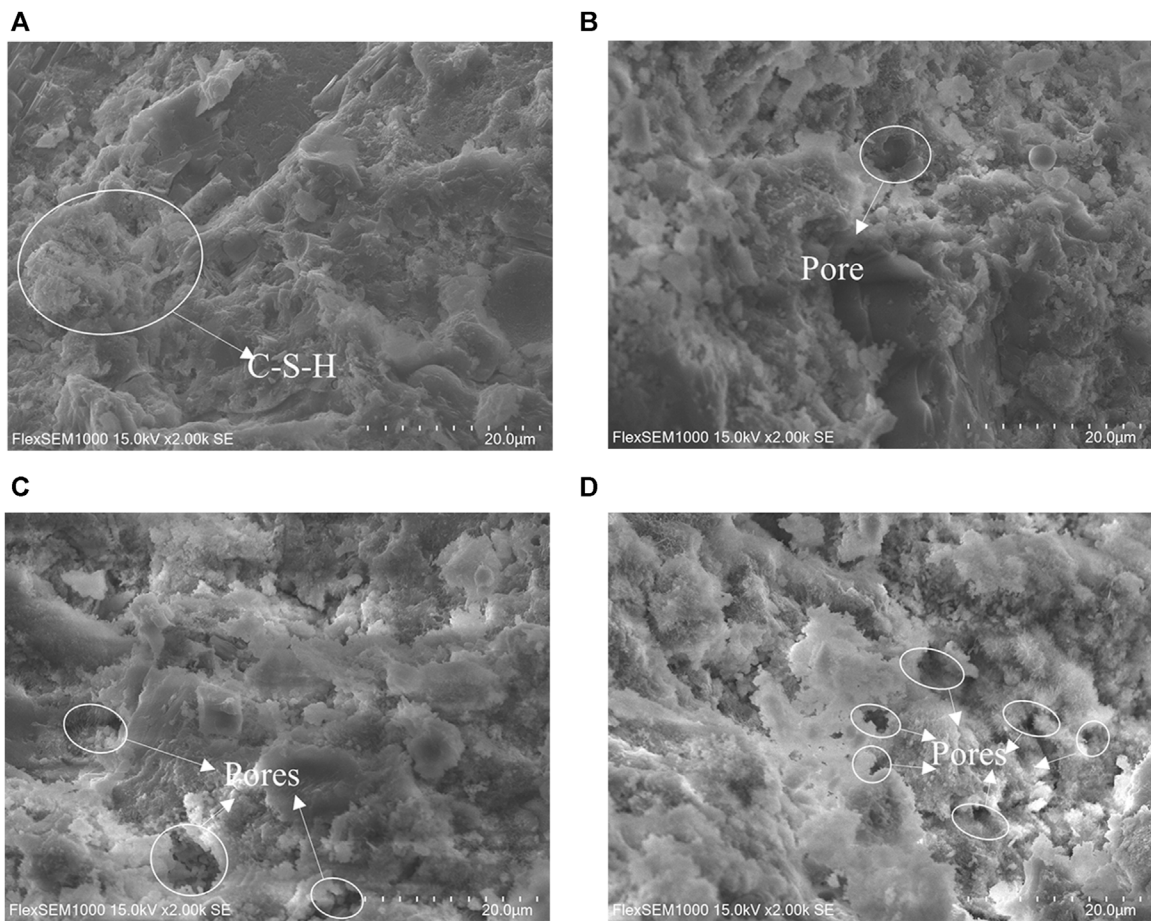
FIGURE 10
SEM images of thermally damaged mortar specimens. **(A)** 20°C, **(B)** 200°C, **(C)** 400°C, **(D)** 600°C.
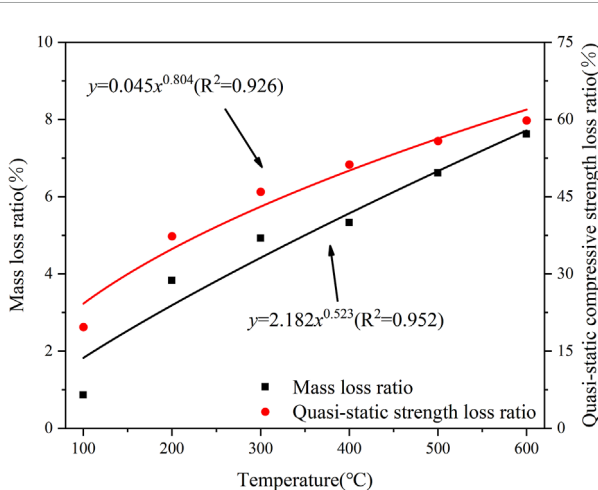

FIGURE 11
Mass and quasi-static compressive strength loss ratio variation of thermally damaged mortar with temperature.

due to the difference of the incident energy (Liu et al., 2020; Yan et al., 2023).

Under different loading conditions, the reflected energy ratio (E_R/E_I) of mortar increased an increase in temperature, as shown in Figure 12A. This was because as thermal treatment temperature increased, the strength of the mortar decreased, resulting in a greater difference in wave impedance between mortar and rod, leading to a worsening energy transfer effect and a larger reflected energy ratio. In terms of numerical value, the reflected energy ratio under static-dynamic loading was larger than that under dynamic loading. This was due to the mortar strength under static-dynamic loading was greater than dynamic loading at same thermal treatment temperature.

Figures 12B, C showed the variation of E_T/E_I and E_A/E_I of mortar with temperature, respectively. From the trend of change, it can be seen that E_T/E_I and E_A/E_I of the mortar under different loading conditions both exhibited a downward trend with increasing temperature. In terms of magnitude, the transmitted energy ratios of the mortar under static-dynamic loading were generally greater than those under dynamic loading, while the absorbed energy ratios

FIGURE 12
Energy proportion variation of thermal mortar with temperature.
(A) E_R/E_I, **(B)** E_T/E_I, **(C)** E_A/E_I.
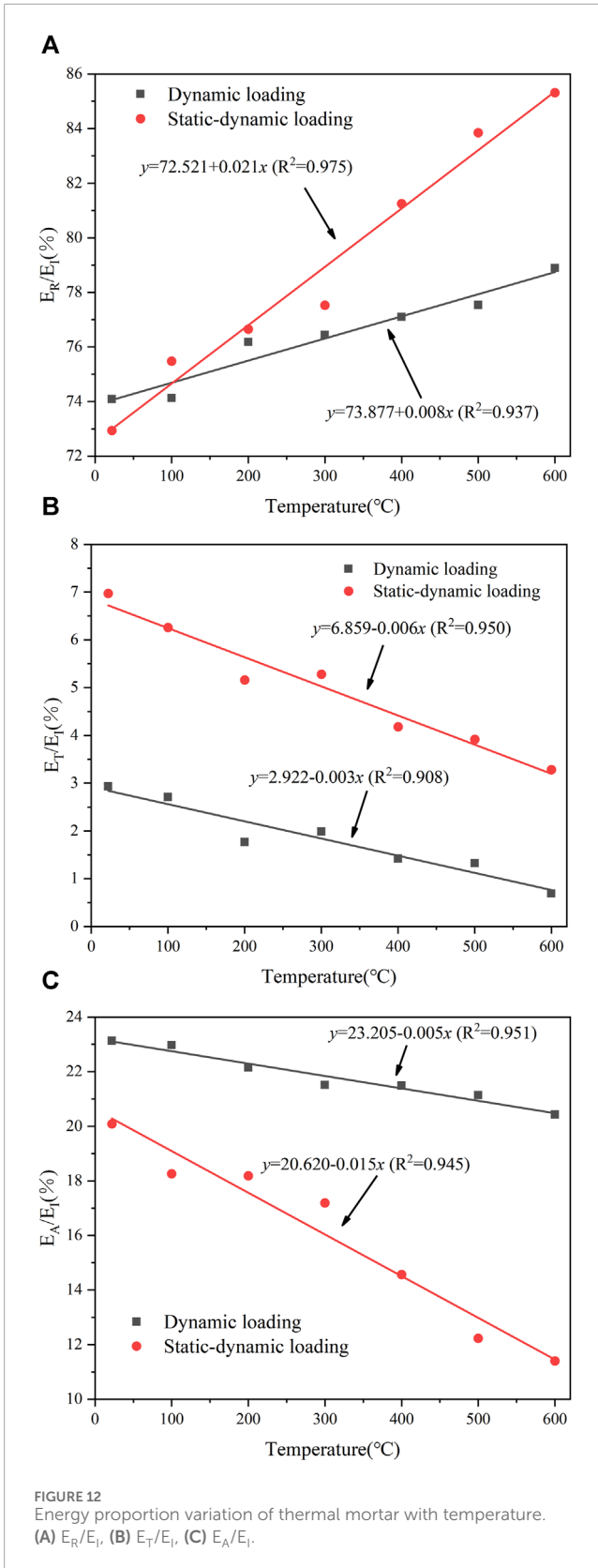
were smaller than those under dynamic loading. This was due to the weakening of mortar strength as the temperature increased, while the pre-applied axial compressive stress helped to enhance its strength.

4 Conclusion

The mechanical properties of thermally damaged mortar specimens under different loading conditions were studied. The findings of this research were intended to offer valuable data for the safety assessment of cement-based structures following a fire event, particularly when subjected to complex loading scenarios. Based on the results, the following conclusions can be drawn:

(1) Under the same loading conditions, compressive strength of thermally damaged mortar decreased as temperature increased. At 600°C, the quasi-static strength loss rate was approximately 60%. *DIF* of the mortar was temperature-sensitive. E_c decreased linearly, while strain rate increased linearly with increasing temperature. It was attributed to the presence of more pores and defects within the mortar's interior following thermal damage, which in return facilitated deformation with increasing temperature.

(2) Under the same thermal treatment temperature, the order of mortar strength under different loading was: static-dynamic loading, dynamic loading and quasi-static loading. In comparison to dynamic loading, mortar subjected to coupled static-dynamic loading exhibited a larger *DIF* and E_c. *DIF* was found to be sensitive to pre-applied axial compressive stress. Additionally, strain rate of mortar under coupled static-dynamic loading was relatively low, ranging from 25 to 30 s^{-1}. It was due to the pre-applied axial pressure before dynamic loading, which helped to compress the pores within the mortar and thus enhance its strength.

(3) Under the same loading condition, increasing temperature resulted in more fragmentation in thermally damage mortar. The increase in pores and microcracks in the mortar was primarily caused by the gradual evaporation of free and bound water, followed by the decomposition of chemical components. Under different loading conditions, the failure mode of thermally damaged mortar was characterized by splitting and tensile failure. Notably, quasi-static loading resulted in the largest broken fragments of mortar, while dynamic loading led to smaller fragments compared to static-dynamic loading. This difference was due to the pre-applied stress, which caused the pore structure to become more compact and thus reduced the degree of mortar crushing.

(4) With increasing temperature, E_R/E_I of mortar increased significantly, while E_T/E_I and E_A/E_I energy ratio decreased. Furthermore, the pre-applied stress had a positive effect on the E_R/E_I and E_T/E_I, while it decreased E_A/E_I. The law governing

the dissipation of energy in mortar was found to be consistent with the strength damage law.

The limitation of this study was that no mortar samples were studied above 600°C. Due to the limitation of instruments and equipment, the maximum thermal temperature of mortar samples only reached 600°C. Subsequently, the dynamical mechanical properties of the cement mortar can be investigated after experiencing higher temperatures.

Data availability statement

The original contributions presented in the study are included in the article/Supplementary Material, further inquiries can be directed to the corresponding author.

Author contributions

CY: Investigation, Methodology, Supervision, Writing–review and editing, Validation. HC: Investigation, Methodology, Supervision, Writing–review and editing, Funding acquisition, Resources. JC: Data curation, Visualization, Writing–original draft. LX: Project administration, Resources, Writing–review and editing, Conceptualization. DY: Supervision, Writing–review and editing.

Funding

Conflict of interest

The authors declare that the research was conducted in the absence of any commercial or financial relationships that could be construed as a potential conflict of interest.

Publisher's note

All claims expressed in this article are solely those of the authors and do not necessarily represent those of their affiliated organizations, or those of the publisher, the editors and the reviewers. Any product that may be evaluated in this article, or claim that may be made by its manufacturer, is not guaranteed or endorsed by the publisher.

References

Aitcin, P. C. (2003). The durability characteristics of high performance concrete: a review. *Cem. Concr. Compos.* 25 (4), 409–420. doi:10.1016/S0958-9465(02)00081-1

Annerel, E., and Taerwe, L. (2009). Revealing the temperature history in concrete after fire exposure by microscopic analysis. *Cem. Concr. Res.* 39 (12), 1239–1249. doi:10.1016/j.cemconres.2009.08.017

Bamonte, P., Gambarova, P. G., and Sciarretta, F. (2021). Thermo-mechanical properties and stress-strain curves of ordinary cementitious mortars at elevated temperatures. *Constr. Build. Mater.* 267, 121027. doi:10.1016/j.conbuildmat.2020.121027

Bi, J., Liu, P. F., and Gan, F. (2020). Effects of the cooling treatment on the dynamic behavior of ordinary concrete exposed to high temperatures. *Constr. Build. Mater.* 248, 118688. doi:10.1016/j.conbuildmat.2020.118688

Biolzi, L., Cattaneo, S., and Rosati, G. (2008). Evaluating residual properties of thermally damaged concrete. *Cem. Concr. Compos.* 30 (10), 907–916. doi:10.1016/j.cemconcomp.2008.09.005

Chen, J., Zhao, C., Ding, F., and Xiang, P. (2019). Experimental study on the seismic behavior of precast concrete column with grouted corrugated sleeves and debonded longitudinal reinforcements. *Adv. Struct. Eng.* 22 (15), 3277–3289. doi:10.1177/1369433219858451

Chen, M., Wang, Y., Zhang, T., and Zhang, M. (2023). Microstructural evolution and dynamic compressive properties of engineered cementitious composites at elevated temperatures. *J. Build. Eng.* 71, 106519. doi:10.1016/j.jobe.2023.106519

Chen, S. G., Zhang, H. M., Wang, L., Yuan, C., Meng, X. Z., Yang, G. S., et al. (2022). Experimental study on the impact disturbance damage of weakly cemented rock based on fractal characteristics and energy dissipation regulation. *Theor. Appl. Fract. Mech.* 122, 103665. doi:10.1016/J.TAFMEC.2022.103665

Chen, Y., Li, X., and Du, H. (2023). A review of high temperature properties of cement based composites: effects of nano materials. *Mater. Today Commun.* 35, 105954. doi:10.1016/j.mtcomm.2023.105954

Cree, D., Green, M., and Noumowé, A. (2013). Residual strength of concrete containing recycled materials after exposure to fire: a review. *Constr. Build. Mater.* 45, 208–223. doi:10.1016/j.conbuildmat.2013.04.005

Dai, F., Huang, S., Xia, K., and Tan, Z. (2010). Some fundamental issues in dynamic compression and tension tests of rocks using split hopkinson pressure bar. *Rock Mech. Rock Eng.* 43 (6), 657–666. doi:10.1007/s00603-010-0091-8

Deng, Z., Huang, H., Ye, B., Xiang, P., and Li, C. (2020). Mechanical performance of RAC under true-triaxial compression after high temperatures. *J. Mater. Civ. Eng.* 32 (8). 04020194. doi:10.1061/(ASCE)MT.1943-5533.0003231

Deng, Z. H., Huang, H. Q., Ye, B. L., Wang, H. P., and Xiang, P. (2020). Investigation on recycled aggregate concretes exposed to high temperature by biaxial compressive tests. *Constr. Build. Mater.* 244, 118048. doi:10.1016/j.conbuildmat.2020.118048

Du, S., Zhang, Y. C., Sun, Q., Gong, W. Y., Geng, J. S., and Zhang, K. J. (2018). Experimental study on color change and compression strength of concrete tunnel lining in a fire. *Tunn. Undergr. Space Technol. incorporating Trenchless Technol. Res.* 71, 106–114. doi:10.1016/j.tust.2017.08.025

Faisal, A., Waleed, A., and Qais, F. (2018). Effect of high temperature and type of cooling on some mechanical properties of cement mortar. *MATEC Web Conf.* 162, 02010. doi:10.1051/matecconf/201816202010

Gao, S., Li, W., Yuan, K., and Rong, C. (2023). Properties and application of thixotropic cement paste backfill with molybdenum tailings. *J. Clean. Prod.* 391, 136169. doi:10.1016/j.jclepro.2023.136169

Hertz, K. D. (2005). Concrete strength for fire safety design. *Mag. Concr. Res.* 57 (8), 445–453. doi:10.1680/macr.2005.57.8.445

Jeyaprabha, B., Elangovan, G., and Prakash, P. (2016). Effects of elevated temperature and water quenching on strength and microstructure of mortars with river sand substitutes. *Constr. Build. Mater.* 114, 688–698. doi:10.1016/j.conbuildmat.2016.03.189

Jiang, Y., Zhang, S., Xue, G., and Wang, W. (2023). Compressive behavior of rubberized concrete under high strain rates. *Structures* 56, 104983. doi:10.1016/j.istruc.2023.104983

Khoury, G. A. (2000). Effect of fire on concrete and concrete structures. *Prog. Struct. Eng. Mater.* 2 (4), 429–447. doi:10.1002/pse.51

Li, Q., Qing, T. D., Huang, C., Yu, B. B., Gao, Z. H., and Wang, K. (2023). Dynamic and damage characteristics of mortar composite under impact load. *KSCE J. Civ. Eng.* 27 (3), 1383–1395. doi:10.1007/S12205-023-1709-1

Li, Z. W., Xua, J. Y., and Baia, E. (2012). Static and dynamic mechanical properties of concrete after high temperature exposure. *Mater. Sci. Eng. A* 544, 27–32. doi:10.1016/j.msea.2012.02.058

Liu, P. F., Zhou, X. P., Qian, Q. H., Berto, F., and Zhou, L. S. (2020). Dynamic splitting tensile properties of concrete and cement mortar. *Fatigue & Fract. Eng. Mater. Struct.* 43 (4), 757–770. doi:10.1111/ffe.13162

Lu, X., Lu, X. Z., Guan, H., and Ye, L. P. (2013). Collapse simulation of reinforced concrete high-rise building induced by extreme earthquakes. *Earthq. Eng. Struct. Dyn.* 42 (5), 705–723. doi:10.1002/eqe.2240

Luo, X., Cheng, J., Xiang, P., and Long, H. (2020). Seismic behavior of corroded reinforced concrete column joints under low-cyclic repeated loading. *Archives Civ. Mech. Eng.* 20 (2), 40–20. doi:10.1007/s43452-020-00043-z

Michał, K., Paweł, B., Łukasz, M., and Jerzy, M. (2023). Comparison of selected blasting constitutive models for reproducing the dynamic fragmentation of rock. *Int. J. Impact Eng.* 173, 104484. doi:10.1016/J.IJIMPENG.2022.104484

Min-Ho, G., and Jung, S.-J. (2006). An experimental study on the characteristics of compressive strength in cement mortar under high temperature conditions in an early age. *J. Archit. Inst. Korea Struct. Constr.* 22 (3), 103–110. www.dbpia.co.kr.

Mukesh, S. T., and Shashank, K. (2019). Impact of passive fire protection on heat release rates in road tunnel fire: a review. *Tunn. Undergr. Space Technol. incorporating Trenchless Technol. Res.* 85, 149–159. doi:10.1016/j.tust.2018.12.018

Padmanabha, V., Schäfer, F., Rae, A. S. P., and Kenkmann, T. (2022). Dynamic split tensile strength of basalt, granite, marble and sandstone: strain rate dependency and fragmentation. *Rock Mech. Rock Eng.* 56 (1), 109–128. doi:10.1007/S00603-022-03075-4

Patrick, B., and Pietro, G. G. (2014). Properties of concrete subjected to extreme thermal conditions. *J. Struct. Fire Eng.* 5 (1), 47–62. doi:10.1260/2040-2317.5.1.47

Schrefler, B. A., Brunello, P., Gawin, D., Majorana, C. E., and Pesavento, F. (2002). Concrete at high temperature with application to tunnel fire. *Comput. Mech.* 29 (1), 43–51. doi:10.1007/s00466-002-0318-y

Shu, R., Huang, L., Zhi, X., Han, Z., Lai, Y., Li, H., et al. (2022). Damage characteristic of thermal shock on the physical and dynamic compressive properties of granite. *Geofluids* 2022, 1–12. doi:10.1155/2022/1623883

Shuai, W., Xu, Y., Xia, K., and Tong, T. (2020). Dynamic fragmentation of microwave irradiated rock. *J. Rock Mech. Geotechnical Eng.* 13 (2), 300–310. doi:10.1016/j.jrmge.2020.09.003

Son, T. P., and William, P. (2014). Effects of high temperature on the microstructure of cement mortar. *Appl. Mech. Mater.* 3207 (556-562), 969–972. doi:10.4028/www.scientific.net/AMM.556-562.969

Stoyanov, V., Petkova, V., Kostova, B., and Kaljuvee, T. (2023). Thermal investigation on high temperature treatment of cement mortars with high content of marble powder. *IOP Conf. Ser. Mater. Sci. Eng.* 1276 (1), 012005. doi:10.1088/1757-899X/1276/1/012005

Xiong, L. X., and Chen, C. (2020). Tests on the mechanical properties of corroded cement mortar after high temperature. *Civ. Eng. J.* 6 (3), 459–469. doi:10.28991/cej-2020-03091483

Xu, Z., Hao, H., and Li, H. N. (2011). Experimental study of dynamic compressive properties of fibre reinforced concrete material with different fibres. *Mater. Des.* 33, 42–55. doi:10.1016/j.matdes.2011.07.004

Yan, Z., Dai, F., Wang, L., Jin, J., and Wang, J. (2023). Dynamic mode II fracture mechanism of rocks using a novel double-edge notched flattened Brazilian disc specimen in the split Hopkinson pressure bar tests. *Eng. Fract. Mech.* 290, 109530. doi:10.1016/J.ENGFRACMECH.2023.109530

Yao, W., Liu, H.-W., Xu, Y., Xia, K., and Zhu, J. (2017). Thermal degradation of dynamic compressive strength for two mortars. *Constr. Build. Mater.* 136, 139–152. doi:10.1016/j.conbuildmat.2017.01.048

Yao, W., Xu, Y., Wang, W., and Kanopolous, P. (2016). Dependence of dynamic tensile strength of longyou sandstone on heat-treatment temperature and loading rate. *Rock Mech. Rock Eng.* 49 (10), 3899–3915. doi:10.1007/s00603-015-0895-7

Yazıcı, Ş., Gözde İnan Sezer, and Şengül, H. (2012). The effect of high temperature on the compressive strength of mortars. *Constr. Build. Mater.* 35, 97–100. doi:10.1016/j.conbuildmat.2012.02.082

Yin, T., Bai, L., Li, X., Li, X., and Zhang, S. (2018). Effect of thermal treatment on the mode I fracture toughness of granite under dynamic and static coupling load. *Eng. Fract. Mech.* 199, 143–158. doi:10.1016/j.engfracmech.2018.05.035

Yu, Z., Meng, Y., Mo, K. H., Liu, H., and Ling, T. C. (2023). Influences of w/c and CO2 curing duration on the high temperature properties of cement pastes. *J. Build. Eng.* 69, 106293. doi:10.1016/j.jobe.2023.106293

Zhang, B., Bicanic, N., Pearce, C. J., and Balabanic, G. (2000). Residual fracture properties of normal- and high-strength concrete subject to elevated temperatures. *Mag. Concr. Res.* 52 (2), 123–136. doi:10.1680/macr.2000.52.2.123

Zhang, X. F., Huang, B. F., and Ma, X. F. (2023). Dynamic compressive impact tests of building sandstone with a large split hopkinson pressure bar. *J. Build. Eng.* 67, 106023. doi:10.1016/J.JOBE.2023.106023

Zhao, Y., Bi, J., Zhou, X. P., and Huang, Y. S. (2019). Effect of high temperature and high pressure of water on micro-characteristic and splitting tensile strength of gritstone. *Front. Earth Sci.* 7. doi:10.3389/feart.2019.00301

Zheng, T., Zhang, Q., Yuan, L., Liu, Z., Niu, L., and Wang, X. (2023). Shape characteristics and crushed law of deep sandstone impact crushed blocks based on digital reconstruction. *Int. J. Impact Eng.* 174, 104525. doi:10.1016/J.IJIMPENG.2023.104525

Zhou, Y. X., Xia, K., Li, X. B., Li, H. B., Ma, G. W., Zhao, J., et al. (2012). Suggested methods for determining the dynamic strength parameters and mode-I fracture toughness of rock materials. *Int. J. Rock Mech. Min. Sci.* 49, 105–112. doi:10.1016/j.ijrmms.2011.10.004